CURRENT SCIENCE AND TECHNOLOGY (CST)
VOL. 02, ISSUE 1, 1 – 11
DOI: https://doi.org/10.15282/cst.v2i1.7371

ORIGINAL ARTICLE

Synthesis of Mxene-PVDF Composite Nanofiber Cloth

Sugaseni Sounderajan[1,*], Jin Kiong Ling[1,2] , Rajan Jose [1,2]

[1]Faculty of Industrial Sciences and Technology, Universiti Malaysia Pahang, 26300 Pahang, Malaysia
[2]Center for Advanced Intelligent Materials, Universiti Malaysia Pahang, 26300 Pahang, Malaysia

ABSTRACT – Electrospinning is a versatile and low-cost technology in producing polymer fibers with diameter ranging from a few microns to nanometers, which can be suitably twisted to make yarns. The aim of this research is to synthesize MXENE-incorporated poly(vinylidene fluoride) (MXENE@PVDF) nanofiber using electrospinning method. The effect of MXENE-to-PVDF ratio on the properties of the nanofiber is studied to investigate its suitability as the separator for energy storage devices. The formation of MXENE@PVDF nanofibers through electrospinning method was confirmed through Field-Emission Scanning Electron Microscope (FESEM). X-ray powder diffraction spectroscopy (XRD) was utilized to study the sample crystallinity and to confirm presence of MXENE. The presence of MXENE was further validated through observing the interaction of functional group between MXENE and PVDF through Fourier-transform infrared spectroscopy (FTIR). The main purpose of this project is to formulate a polymeric solution using MXENE and PVDF with desirable rheological properties such that a polymeric mat can be synthesized using electrospinning.

ARTICLE HISTORY
Received: 27th Jan 2022
Revised: 14th June 2022
Accepted: 23rd Dec 2022

KEYWORDS
Mxene
PVDF
Electrospinning
Nanofiber

INTRODUCTION

The coronavirus 2019 (COVID-19) epidemic was declared as a public health emergency in December 2019 by the World Health Organization, with its devastating effect felt in almost all counties in the planet Earth. With the need to continuously track and contain the epidemic as a measure of control, capability to continuously monitor the health and location of close contact signified the vitality in developing wearable electronics, triggering huge impact on the Smart Clothing industry[1]. In fact, the global market value of Smart Clothing market recorded USD 110.7 million in 2020 and is projected to be USD 199.2 million by 2026, with a CAGR of 74.0 percent between 2021 and 2026 [2]. One of the main driving factors for such growth is the emerging trend of electronics miniaturization as well as the rising convergence of smart textiles with wearable devices.

Electronic textiles are referred to the textile structure which are having electrical functionality same as the electronics, while physically behaving as a textile. E-textiles offer many benefits, including being foldable, flexible, low-cost, lightweight, and stretchable. It is crucial to take note that these functionalities need to be retained after repeated washing[3]. Undeniably, prodigious research endeavour has been directed into enhancing the production process, functionality, and performance of electronic textile (E-textile). Even though E-textiles are currently not commercially and economically feasible due to complicated production process and few aesthetic issues, continuous research efforts would soon see an increase in popularity for applications such as disposable electronic, sensor, flexible, military, real-time health tracking, exercise training, medical care and others.

Natural polymers are a good choice in fibre processing because of the advantages they offer, including resemblance to host tissue, rapid penetration into wounded site, biocompatibility, biodegradation, ability to be degraded by enzymes, and the capability to react with various biological structures[4]. Numerous polymers had been made into yarns, such as polyamide polyester, nylon, vinyon, olefin fiber, polyurethane, elastolefin, polyethylene.

Polyvinylidene fluoride (PVDF) has sparked considerable as among the most promising, it has received a lot of attention. choices for wearable gadgets or smart fabrics due to its flexibility and unique electroactive characteristics. PVDF's molecular structure and organisation result in distinct chain conformations, allowing three different crystal polymorphs which are, (α, β, and γ). Because of its all-trans conformation, β phase crystal structure also has some strong electroactivity and mechanical qualities, allowing for unidirectional polarisation. As a result, β crystal formation via stretching (drawing), compression, annealing, and electrical poling has been actively reported to optimise those features and potential for numerous applications such as sensors and energy harvesters. Inducing highly ordered PVDF interphase by introducing nano-fillers with strong interactions with PVDF is one of the simplest and most efficient ways to improve β phase fraction. PVDF with the nanocomposite film with 5 wt% SiO2 had a β phase fraction of 6%, resulting in a greater dielectric constant and piezoelectric behaviour than PVDF/GeO2 and control PVDF films (58% and 33& respectively). However, the bulk of research to date has been on the form of film or electro-spun mat (nanofiber), which have limitations in being employed as a smart textile due to poor mechanical qualities and dimension mismatch for textile application. As

*CORRESPONDING AUTHOR | Sugaseni S. | ✉ sugasinisounderajan@gmail.my

a result, fibres with high mechanical and electroactive qualities are required to unlock the full potential of functional fibres and next-generation smart textiles [5].

Electrospinning is a simple method; it has grown in popularity due to its small fibre diameter and unique physical and chemical properties. As a result, non-woven cloth processing on a nanoscale can be used to manufacture electrospinning. Those non-woven fabrics are usually which is smaller than 1m (meter) and can be easily gathered by the electrospinning process.

In terms of downsizing, usefulness, and comfort, the introduction of electronics into wearable products has made great progress. These e-textiles offer a wide range of applications, including individual health tracking, high-performance apparel, wearable screens, and a new class of portable gadgets are all on the horizon. Power sources that are small and light, stretchable, and wearable, such as batteries and supercapacitors are in high demand as an essential component of various applications. The ideal wearable power sources would be constructed as breathe through textiles with stretchability (as an example: mechanical resilience) that conformed with relation to the curved surface with maintained its purpose throughout body movement. Supercapacitors, as one sort of power source, have higher power density, superior reversibility, and has a long-life cycle [6] .

METHODOLOGY

Preparation of Mxene

MAX (Ti3AlC2) and HF was mixed in a weight ratio of 3/60. The mixture was etched for 72 hours while magnetically stirred. The bottle was stirred in oil as an oil bath at temperature of 30°C with stri speed of 133 RPM. After 72 hours of etching, the aluminium element was removed from the mixture solution and then add deionized water washing process. The centrifugation was set at speed of 3890 rpm and duration of 8 minutes. The washing process was repeated until the supernatant reaches pH7. Then the Mxene added with the DMSO and let it to be stirred for overnight. The Mxene was sonicated for 6 hours, followed by vacuum filtration and drying in oven for overnight at 60oC. The obtained Mxene powder was collected and used without further purification.

Preparation of solution

To prepare the electrospinning polymeric solution, 0.59 g of PVDF pellet with molecular weight of 265,000 were added to 2.2 ml DMF, termed as solution A. The mixture was magnetically stirrer for 2 hours in water bath of 45oC. While dissolving PVDF solution, 0.1 wt% of MXene was dissolved into 0.3 ml of DMF. The solution B was stirred for 1 hour, followed by 15 minutes ultrasonication to homogeneously distribute MXENE throughout the DMF solvent. The solution B was then mixed into solution A, followed by magnetic stirring for another hour. Similar process was repeated to prepare MXENE@PVDF polymer solution with 0.5 and 1.0 wt% of MXENE.

Figure 1. Prepared Mxene solution & PVDF solution

Electrospinning

After the solution fully dissolve for 1 hour. The solution was draw up as 2ml in the syringe of 5ml. Then, insert the needle with the size of 26G x 1/2 (0.45mm x 13mm). the draw up syringe were insert on the electrospinning machine. The voltage current pass was connected to the collector and needle. The polymer solution wase pumped into the tip of the needle. The setting was set as volume 1.50ml and rate at 1.03 ml/H. Through applying high voltage to the device of 10-15 kV, an electric field was formed between the tip of the needle and the collector plate. The collector plate was covered with aluminium foil and non-woven Spunbond Fabric. As the power of the electric field overcomes the surface tension in a liquid droplet, the droplet distorts, creating the so-called Taylor cone. The distortion causes an electrically altered jet injection to travel into the collector which on the non-woven Spunbond Fabric. Thus, resulting in the formation of thin fibres. Polymer fibres that are matched are created when a spinning collector is used.

Figure 2. Electrospinning setup

Field Emission Scanning Electron Microscopy (FESEM)

At magnifications ranging from 10x to 300,000x and with a nearly infinite depth of field, field emission scanning electron microscopy (FESEM) delivers topographical and elemental information. Field emission scanning electron microscopy (FESEM) delivers crisper, less electrostatically distorted pictures with spatial resolution down to 1 1/2 nanometers – three to six times better than conventional scanning electron microscopy (SEM). The capacity to investigate contaminated patches in smaller areas at electron accelerating voltages suitable with energy dispersive spectroscopy (EDS). Low-kinetic-energy electrons penetrate less deeply, bringing them closer to the material's surface. High-quality, low-voltage photographs with little sample electrical charging (accelerating voltages ranging from 0.5 to 30 kilovolts). There is no need to apply conducting coatings on insulating materials[7]. In this study, all samples were coated with a thin layer of platinum through sputtering coating for 5 minutes to ensure no surface space charge formation on the surface of the samples. The samples were observed at an accelerating voltage of 30 kV, with a stage height of 10 mm and magnification of x(value).

X-ray Diffraction Analysis (XRD)

Basically, examination of the crystal structure in XRD analysis is used to determine the crystalline phases contained in a material and hence give chemical composition information. The stages are identified by comparing the obtained data to that in reference databases. Minerals, polymers, corrosion products, and unknown materials can all benefit from X-ray diffraction. In most situations, the materials tested at Element are evaluated utilising powder diffraction on finely powdered particles[8]. In this study, the samples were irradiated with electron beam from Cu Kα ($\lambda = 0.15406$ nm) from 5-80o, with a step size of 0.02º.

Fourier Transform Infrared spectroscopy (FTIR)

The technique of Fourier transform infrared spectroscopy (FTIR) is used to obtain an infrared spectrum of absorption or emission of a solid, liquid, or gas. FTIR may be used to capture high-resolution spectral data across a wide range, typically between 5000 and 400 cm1 for mid-IR wavelengths and between 10,000 and 4000 cm1 for near-IR wavelengths [9].

Electrochemical Analysis

The synthesized polymeric mat was cut into circular shape with 15mm diameter and the weight of the electrode was measured using a weighing machine. Prior to CR2032 coin cell fabrication, the prepared electrode was immersed in 2M KOH electrolyte for 15 minutes to improve electrolyte intake. Meantime, the separator was prepared by cutting glass microfibre filter membrane into circular disc with diameter of 17 mm. Then, one of the submerged electrodes was placed in to bottom of cap. The separator membrane was placed on top of the electrode two additional drops of 2M KOH was added. The counter electrode was placed above the separator membrane, follow by a metal spacer, conductive spring, and top cap. Finally, the coin cell was crimped at a force of 5 ton.

EXPERIMENTAL RESULTS

The morphological images of the synthesized fiber in Figure 3 were taken at magnification of 5000x. All samples showed morphology of homogenous continuous beadless nanofiber. In general, the whipping and stretching forces of the electrospinning process could induce the β-phase in PVDF (responsible for piezoelectricity)[10] which could be further improved by high-speed collecting for fibre alignment. The Fourier transform infrared (FTIR) and X-ray diffraction (XRD) spectra were used to identify the phases in the fibres. The diameter of nanofiber increases with the wt% of Mxene. The average diameter of the pure PVDF is measured to be 137nm, 143nm for 0.1 wt% of MXENE, 171nm for 0.5 wt% MXENE and 237nm for 1 wt% of MXENE. Therefore, it can be concluded that the higher the percentage content of Mxene, the larger the diameter of nanofiber.

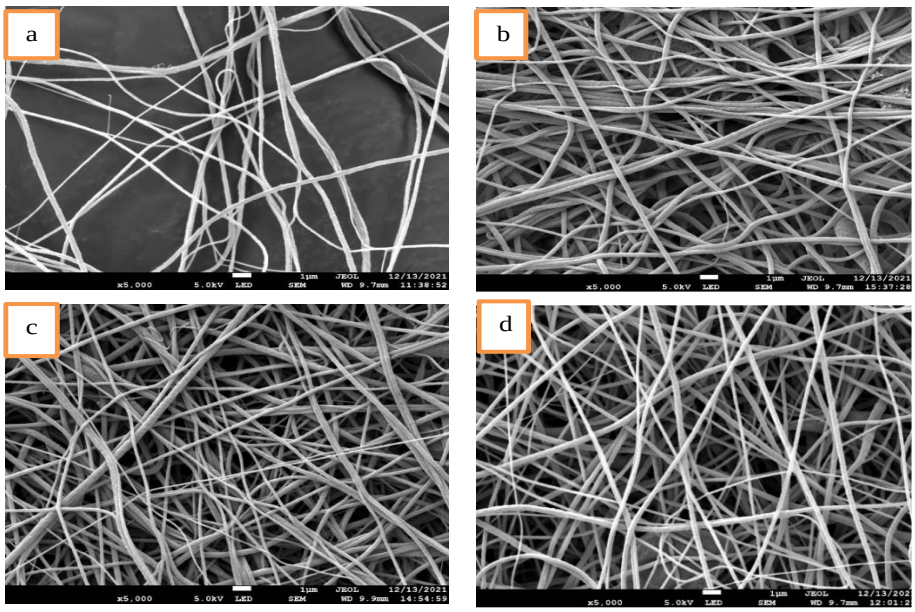

Figure 3. The FESEM image of fiber at magnification of x5000 a) Pure without Mxene, (b)0.1wt% of Mxene, (c) 0.5wt% of Mxene, (d) 1wt% of Mxene

Crystal Structure of the Nanofiber (XRD Ananlysis)

The crystal structures of all samples were studied using XRD analysis. The Figure 4 shows XRD result and the peak's intensity difference between pure PVDF, 0.1wt%, 0.5wt%, and 1wt% of Mxene. The peak at crystal plane (110) shows the present of PVDF. Compare the intensity of pure PVDF at crystal plane (110), considering the minute amount of Mxene used compared to PVDF, the peak of PVDF is higher compared to that of Mxene. The presence of MXene can be confirmed from three distinct peaks detected at 2θ= 9.7°, 19.1°, and 39°, corresponding to the (001), (020), and (006) crystal planes of MXENE, respectively. Two other prominent peaks can be observed at 2θ =18° (020) and 2θ = 22° (110), which corresponded to PVDF used in the fiber. In overall, samples diffractograms consist of a dominating peak at 2 θ =20.2° (200/110), 20.3° (200/110), and 20.4° (200/110), all of which were ascribed to the β -phase of PVDF. These peaks are prominent throughout all the diffractograms, indicating the formation of a β-phase PVDF in all the samples. The molecular interaction between the PVDF and the solvent is an essential parameter in enhancing the crystallized-phase in PVDF. Adopting DMF as the solvent, molecular interactions include dipolar interactions between C=O in DMF and CH2 – CF2 PVDF as well as the existence of weak hydrogen bonding C=O....H– C, both of which break the inter-chain forces of solid PVDF and eventually dissolve it. At low temperatures, the reaction energy between polymer molecular chains is larger than the reaction energy of the polymer-solvent interaction, therefore the crystalline area of the PVDF remains essentially interactive and swelling occurs when the solvent enters the amorphous region. The reaction energy of polymer chain reduced and the solvent enter the crystalline area at high temperatures, resulting in total or partial dissolution.

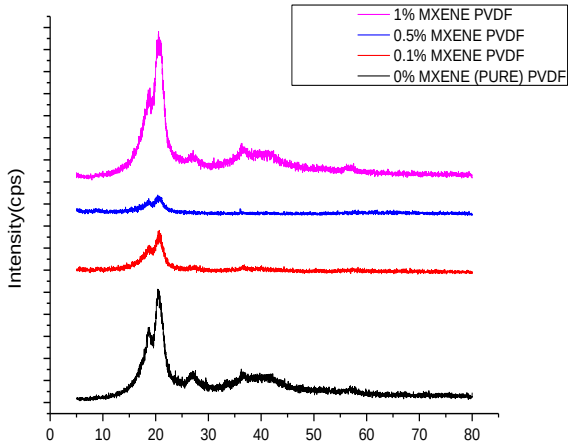

Figure 4. XRD spectral trends of the synthesized Nanofiber of Pure PVDF, 0.1wt%, 0.5wt%, 1wt% of Mxene.

Fourier Transform Infrared Spectroscopy (FTIR)

The FTIR is used to identify the interaction between different molecules. The higher the wt% of Mxene, the lower the Transmittance (%). FTIR results for nanofiber confirmed the presence of Mxene and PVDF containing functional groups on the aromatic, aromatic-mono-substituted, aromatic amide, primary alcohol and carboxylic acid. MXenes have high hydrophilicity for surface groups with –OH, =O, and –F terminations. There is a high possibility that increasing the amount of MXENE will change the bond vibrational energy of functional group. MXENE is hydrophilic and would adsorb moisture. The Mxene interact with PVDF. The interaction of Mxene in PVDF the different in peak intensity. The samples absorb more moisture when percentage of Mxene content increase. While the Figure 5 shows the comparisons of FTIR graph of all the samples.

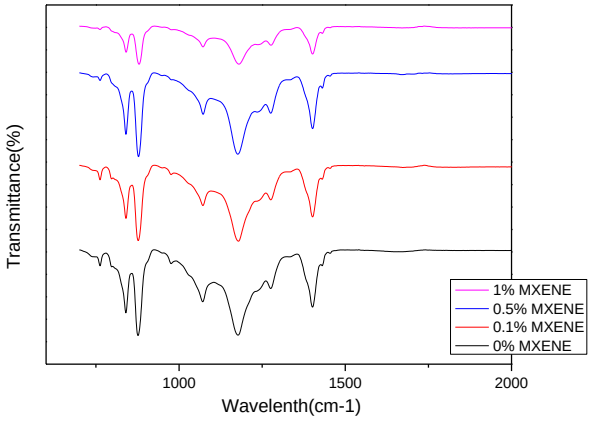

Figure 5. FTIR of pure PVDF, 0.1wt%, 0.5wt%, 1wt% of Mxene.

Table 1. Shows the wavelength and Functional Group of the FTIR graph

Samples (wt%)	Wavelength range(cm^{-1})	Functional Group
0%	840.04 cm^{-1}	Aromatic compound
	876.46 cm^{-1}	Aromatic (Ar-C)
	762.28 cm^{-1}	Aromatic mono-substituted (C-C)
	1071.19 cm^{-1}	Primary alcohol (C-O)
	1177.50 cm^{-1}	Aromatic Amine (C-N)
	1275.71 cm^{-1}	Carboxylic Acid (C-O)
	1401.46 cm^{-1}	Carboxylic Acid (C=O)
0.1%	762.27 cm^{-1}	Aromatic mono-substituted(C-C)
	840.30 cm^{-1}	Aromatic compound
	877.01 cm^{-1}	Aromatic (Ar-C)
	1071.72 cm^{-1}	Primary alcohol (C-O)
	1178.55 cm^{-1}	Aromatic Amine (C-N)
	1275.85 cm^{-1}	Carboxylic Acid (C-O)
	1401.70 cm^{-1}	Carboxylic Acid (C=O)
0.5%	762.31 cm^{-1}	Aromatic mono-substituted (C-C)
	840.23 cm^{-1}	Aromatic compound
	877.95 cm^{-1}	Aromatic (Ar-C)
	1072.29 cm^{-1}	Primary alcohol (C-O)
	1176.66 cm^{-1}	Aromatic Amine (C-N)
	1275.68 cm^{-1}	Carboxylic Acid (C-O)
	1401.73 cm^{-1}	Carboxylic Acid (C=O)
1%	840.73 cm^{-1}	Aromatic compound
	879.54 cm^{-1}	Aromatic (Ar-C)
	1072.09 cm^{-1}	Primary alcohol (C-O)
	1401.59 cm^{-1}	Carboxylic Acid (C=O)
	1180.20 cm^{-1}	Aromatic Amine (C-N)

Electrochemical Performance Analysis

To study the electrochemical performance of the synthesized samples as the electrode for symmetry aqueous electrolyte capacitor, three analyses were carried out - cyclic voltammetry (CV), galvanostatic charge-discharge (CDC), and Electrochemical Impedance Spectroscopy (EIS). The current that flows through an electrochemical cell when the voltage is swept through a voltage range is shown by CV. The CV experiment is represented as a plot of applied potential vs current. Capacitance could also be measured using EIS, where the Impedance, Z' (Ω) vs Impedance, Z" (Ω) is plotted (also known as Nyquist plot). CDC is performed by measuring the potential of the cells across the measurement time under a constant applied current.

Cyclic voltammetry is a technique often used to investigate the redox process in electrode systems. Analysing the CV curve yields the electrochemical window of the electrode, the location of redox, and the related peak value. Figure 6 show the Cyclic Voltammetry curve of all the samples at different scan rate. The scan rate used throughout this analysis were 0.05 V/s, 0.075 V/s, 0.1 V/s, 0.25 V/s, and 0.5 V/s. An increase in the slope of current can be observed when the cells were charged near to 1 V, indicating that all samples can only be charged up to 1 V. Further charging the cells to >1 V would eventually cause the samples to degraded, leading to poor cycling stability. Therefore, all the samples were only charged up to 1 V. The absence of redox peak during cathodic and anodic process for all four samples indicate that the charge was stored through non-faradaic surface adsorption process. The CV can also be used to calculate specific capacitance using the expression below:

$$\textit{Specific Capacitance (F/g)} = \frac{area\ under\ the\ curve}{2\ x\ scan\ rate\ x\ voltage\ x\ mass} \qquad (1)$$

Table 2, shows that, the specific capacitance of Sample with Pure Mxene have highest value which is 1430 F/g, at a scan rate of 0.05V/s and voltage of 1V. While the lowest Specific Capacitance is with Pure Mxene which is 22 F/g, at a scan rate of 0.5V/s and voltage of 1V.

Table 2. The value of Specific Capacitance of CV graph

Samples (wt%)	Area under curve	Scan rate(V/s)	Voltage(v)	Mass(g)	Specific Capacitance (F/g)
0%	0.286	0.05	1	2×10^{-3}	1430
	0.284	0.075	1	2×10^{-3}	946.7
	0.286	0.1	1	2×10^{-3}	715
	0.246	0.25	1	2×10^{-3}	246
	0.044	0.5	1	2×10^{-3}	22
0.1%	0.371	0.05	1	3.4×10^{-3}	1091.1
	0.371	0.075	1	3.4×10^{-3}	824.4
	0.366	0.1	1	3.4×10^{-3}	538.2
	0.171	0.25	1	3.4×10^{-3}	100.5
	0.605	0.5	1	3.4×10^{-3}	177.9
0.5%	0.190	0.05	1	4.9×10^{-3}	387.7
	0.219	0.075	1	4.9×10^{-3}	297.9
	0.217	0.1	1	4.9×10^{-3}	221.4
	0.215	0.25	1	4.9×10^{-3}	87.7
	0.232	0.5	1	4.9×10^{-3}	43.8
1%	0.379	0.05	1	$3x\ 10^{-3}$	1263.3
	0.373	0.075	1	$3x\ 10^{-3}$	828.8
	0.373	0.1	1	$3x\ 10^{-3}$	621.6
	0.334	0.25	1	$3x\ 10^{-3}$	248.6
	0.373	0.5	1	$3x\ 10^{-3}$	124

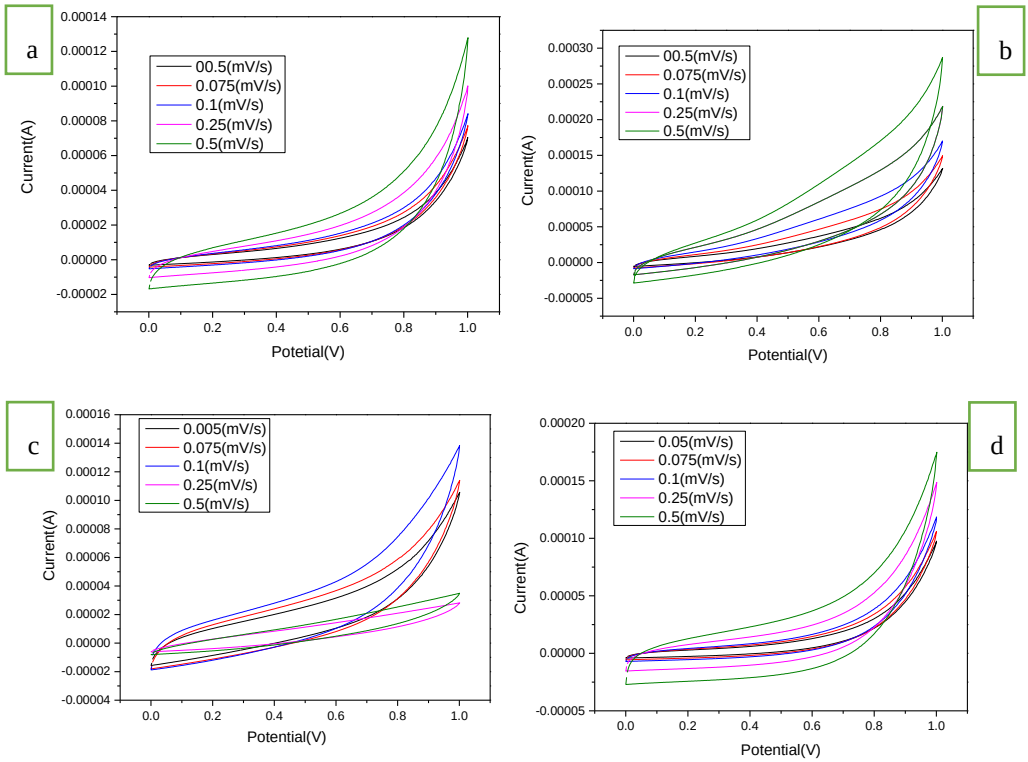

Figure 6. Shows the Cyclic Voltammetry (CV) of (a) Pure PVDF (0wt% of Mxene), (b) 0.1wt% of Mxene (c) 0.5wt% of Mxene (d) 1wt% of Mxene

The charge and discharge behaviour of all samples were analysed under current densities ranging from 0.1A/g to 0.001 A/g. Figure 7 shows the charging and discharging of the samples. The voltage decrease in batteries occurs during discharge. To calculate the IR drop, we have to take the final charging voltage and deducted by the first discharging voltage. The discharge equation is the equation Q=AV (Q=discharge rate, A=area, V=velocity). So, the velocity can be calculated by discharge rate and Area under curve The decrease in Velocity time is caused by numerous factors, which is IR drop, coulombic efficiency and the specific capacitance (F/g). (1) IR drop - The drop in cell voltage caused by current flowing through the internal resistance of the battery. At constant temperature, this component increases with a roughly linear slope at greater discharge rates. (2) Activation polarisation- Refers to the many retarding variables inherent in the kinetics of an electrochemical reaction, such as the work function that ion must overcome at the electrode-electrolyte interface. (3) Concentration polarisation takes into account the resistance encountered by the mass transfer (diffusion) process, which transports ions across the electrolyte from one electrode to another. The IR drop of pure PVDF (0wt% of Mxene) is lower compare to others with the value of -0.08V. Table 3 shows the IR drop values.

IR drop(V) = Final charging voltage - First discharging voltage (2)

Table 3. The value of Specific Capacitance of CV graph

Samples(wt%)	Final charging voltage	First discharging voltage	IR drop(V)
0wt%	-0.52V	-0.44V	-0.08V
0.1wt%	-0.47V	0.23V	-0.71V
0.5wt%	-0.41V	-0.04V	-0.37V
1wt%	-0.46V	0.24V	0.70V

Table 4 shows the value of Coulombic efficiency during charge and discharge. The coulombic efficiency analyses the proportion of charge stored and release during charging and discharging. the highest columbic efficiency was recorded in 0.5wt% of Mxene, followed by pure PVDF, 0.1 wt% and 1 wt%.

$$\textbf{Coulombic efficiency (\%)} = \frac{\text{Charging time}}{\text{Discharging time}} \; \boldsymbol{x\ 100} \qquad (3)$$

Table 4. The value of Coulombic efficiency

Samples(wt%)	Charging time(s)	Discharging Time(s)	Coulombic efficiency (%)
0wt%	11.32	3316.91	0.34
0.1wt%	12.07	3832.93	0.31
0.5wt%	21.62	2015.01	1.07
1wt%	11.78	3369.46	0.34

Table 5 shows the values of specific capacitance. The specific capacitance shows that samples with 0.1wt% has the lowest specific capacitance compared to others while 5wt% of Mxene has the highest specific capacitance.

$$\textbf{Specific Capacitance (F/g)} = \frac{\text{Discharge time x Current density}}{\text{Voltage}} \qquad (4)$$

Table 5. The value of Specific Capacitance

Samples(wt%)	Discharging Time(s)	Current density (A/g)	Voltage (V)	Specific Capacitance (F/g)
0wt%	3316.91	0.001	1	3.3
0.1wt%	3832.93	0.001	1	3.8
0.5wt%	2015.01	0.001	1	2.0
1wt%	3369.46	0.001	1	3.3

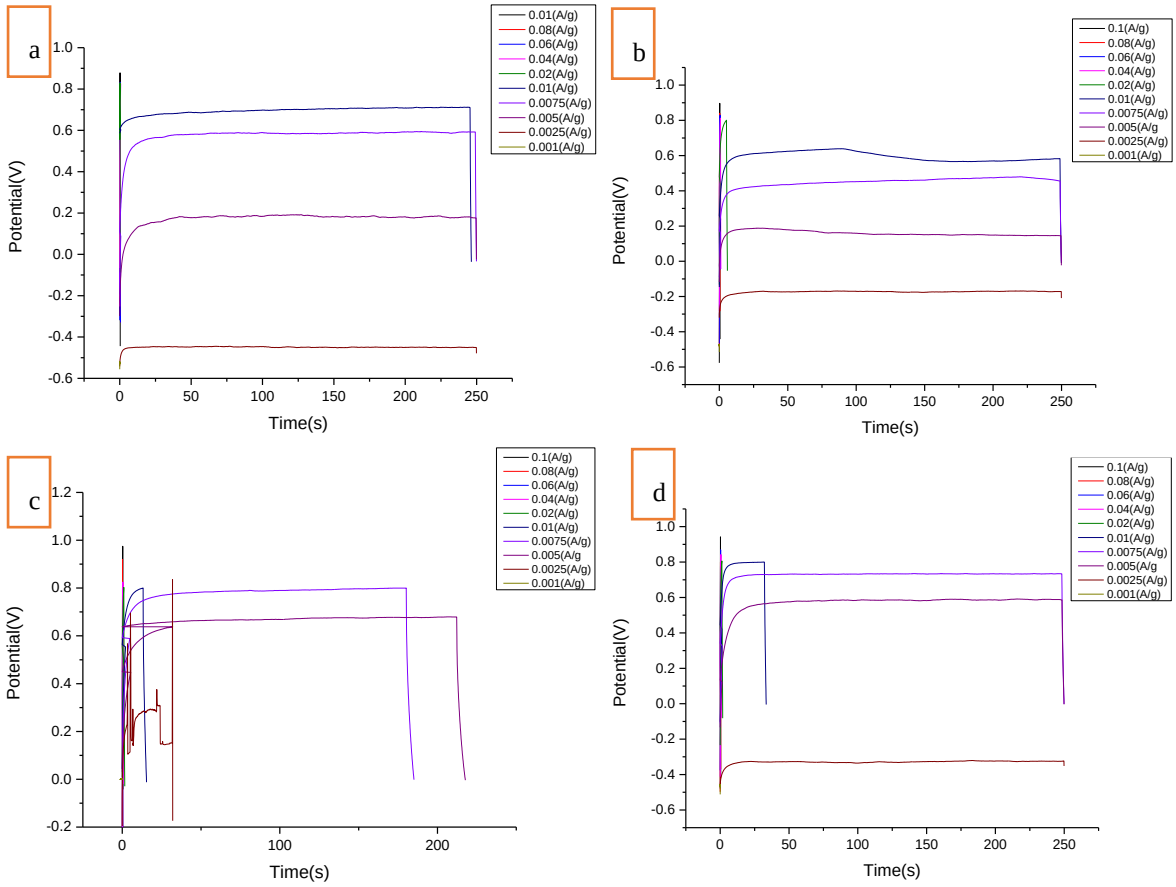

Figure 7. Shows the charging and discharging of (a) Pure PVDF (0wt% of Mxene), (b) 0.1wt% of Mxene (c) 0.5wt% of Mxene (d) 1wt% of Mxene

The Nyquist plot of Mxene@PVDF are shown in Figure 7. All EIS spectra have a semi-circle at the high frequency region and a sloped line at the low frequency region. The diameter of the semi-circle at high frequency region is equivalent to the charge transfer resistance across the electrode. EIS can be used to measure the bulk (RB), and charge transfer (RCT) impedance of the electrodes. The (RCT) can be calculated by RB1 - RB2. the impedances of all four samples are summarized in Figure 8, where sample with 1wt% of Mxene has the lowest RCT value of 1.6 Ω. Table 6 shows the value of RCT.

$$\mathbf{R_{CT}} = R_{B1} - R_{B2} \quad (5)$$

Table 6. Value of RCT and RB

Samples	R_{B1}	R_{B2}	R_{CT}
0% (2mg)	32 Ω	27 Ω	5Ω
0.1%(3.4mg)	15 Ω	5 Ω	10Ω
0.5% (4.9mg)	900 Ω	500 Ω	400Ω
1% (3mg)	51.8 Ω	50.2 Ω	1.6Ω

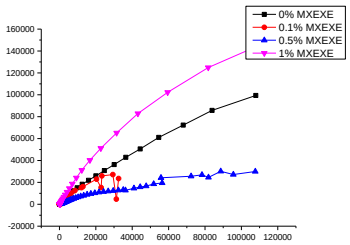

Figure 8. EIS of pure PVDF, 0.1wt%, 0.5wt%, 1wt% of Mxene

CONCLUSION

For this research, composite nanofiber was successfully synthesized using electrospinning method. The effect of different content ratio of MXENE on the electrochemical performance of PVDF nanofibers was studied. The nanofibers cloth was used as a free-standing electrode in coil cell. The morphology of the Mxene@PVDF nanofibers was observed using Field-Emission Scanning Electron Microscope (FESEM). In the FESEM analysis, it was founded that, the diameter of nanofiber increases with the wt% of Mxene. The effect of MXENE content and the crystallinity of Mxene@PVDF solution was analysed using X-ray Powder Diffraction Spectroscopy (XRD). The suitability of Mxene@PVDF as the electrode for energy storage devices was studied by electrochemical measurement (Cyclic-voltammetry (CV), Galvanostatic charge-discharge (CDC), and Electrochemical impedance spectroscopy (EIS) using activated carbon as the electrode.

ACKNOWLEDGEMENT

The authors would like to thank UMP for funding this work.

REFERENCES

[1] Catalysts, F. o. (2020). Retrieved from Global platinum market (2020 to 2025) : https://doi.org/10.1016/j.focat.2020.10.004

[2] Smart Clothing Market and Smart Fabrics Market Size 2020 By Trends Evaluation. (2020). Global Demands, On-Going Trends, Top Countries Data, Opportunity

[3] Balilonda, A. L. (n.d.). Retrieved from Lead-free and electron transport layer-free perovskite yarns: Designed for knitted solar fabrics. Chemical Engineering Journal.

[4] Tamariz, E. &. -R. (2013, June 14). Biodegradation of medical purpose polymeric materials and their impact on biocompatibility.

[5] Lee, J.-E. S.-E.-H., & Chae, H. G. (2021). Polyvinylidene fluoride (pvdf)/cellulose nanocrystal (CNC) nanocomposite fiber and triboelectric textile sensors. Composites Part B: Engineering.

[6] Yue, B. W., & Wallace, G. G. (2021). Polypyrrole coated nylon lycra fabric as stretchable electrode for supercapacitor applications. . Electrochimica Acta.

[7] Field Emission Scanning Electron Microscopy (FESEM). . (n.d.). Retrieved from PhotoMetrics. : https://photometrics.net/field-emission-scanning-electron-microscopy-fesem/.

[8] X-ray diffraction analysis (XRD). (n.d.). Retrieved from Element: https://www.element.com/materials-testing-services/x-ray-diffraction.

[9] White, R. (2020). Chromatography/fourier transform infrared spectroscopy interfaces. Chromatography/Fourier Transform Infrared Spectroscopy and Its Applications, 1–42. https://doi.org/10.1201/9781003066323-1